Molecular organization of Gram-negative peptidoglycan

Lu Gan[a], Songye Chen[a], and Grant J. Jensen[a,b,1]

[a]Division of Biology and [b]Howard Hughes Medical Institute, California Institute of Technology, Pasadena, CA 91125

Edited by M. J. Osborn, University of Connecticut Health Center, Farmington, CT, and approved October 9, 2008 (received for review August 14, 2008)

The stress-bearing component of the bacterial cell wall—a multi-gigadalton bag-like molecule called the sacculus—is synthesized from peptidoglycan. Whereas the chemical composition and the 3-dimensional structure of the peptidoglycan subunit (in at least one conformation) are known, the architecture of the assembled sacculus is not. Four decades' worth of biochemical and electron microscopy experiments have resulted in two leading 3-D peptidoglycan models: "Layered" and "Scaffold", in which the glycan strands are parallel and perpendicular to the cell surface, respectively. Here we resolved the basic architecture of purified, frozen-hydrated sacculi through electron cryotomography. In the Gram-negative sacculus, a single layer of glycans lie parallel to the cell surface, roughly perpendicular to the long axis of the cell, encircling the cell in a disorganized hoop-like fashion.

cell wall | Cryo-EM | sacculus | tomography | cell shape

The organization of peptidoglycan within the sacculus is a longstanding question in microbiology. Although the sacculus completely envelopes the cell, protecting it from osmotic and mechanical lysis, it is also porous, and thus sieves nutrients and small proteins. Sacculi are constantly remodeled, but they are robust enough that they can be purified from cells and still retain their original shape. Early electron microscope images of purified sacculi were difficult to interpret because the images were 2-D projections through heavy metal-stained sacculi (1, 2). Nevertheless the slender appearance of peptidoglycan in thin-sectioned cells (3) and the gaps perpendicular to the polar axis produced by a peptidoglycan-specific endopeptidase (4) lead to the (Circumferential) Layered model (Fig. 1*A*) in which the glycan strands lie in the plane of the cell wall and wrap around the cell. The alternative Scaffold model (5) (Fig. 1*B*) was proposed to fit biochemical data such as pore size and crosslinkage. Various arguments have been made in favor of (6) and against (7) the Scaffold model, but the debate intensified after a recent NMR structure of a synthetic peptidoglycan subunit dimer was interpreted to support the Scaffold model (8). To gain further insight into this issue, we imaged unstained sacculi in 3-D by electron cryotomography (9).

Results and Discussion

Electron Cryotomography of Purified Sacculi. Sacculi isolated from *C. crescentus* strain CB15N and *E. coli* strains MG1655 and XL-10 were vitrified across holey carbon grids in thin (< 100 nm) ice. Whereas the gossamer sacculi were barely discernable in the low-dose, 2-D projection images, they were clearly visible in the 3-D tomograms and resembled flattened cells [Fig. 2 and supporting information (SI) Movie S1 and Movie S2]. In stark contrast to intact cells, the sacculi were flexible and in some positions had radii of curvature less than 20 nm, highlighting how cell shape is not determined by the "rigidity" of the sacculus, but rather the cytosolic turgor (osmotic pressure) pushing the cytoplasmic membrane outward against the saccular "bag". Although the sacculi were flattened, the "upper" and "lower" halves were easily distinguished in cross-sections (see Movie S1 and Movie S2). In this flattened state both halves contained wrinkles (Fig. 3, Movie S1, and Movie S2) that mostly ran perpendicular to the saccular polar axis.

The Sacculus Is a Thin, Single Layer of Peptidoglycan. According to the Scaffold model, the peptidoglycan layer would have to be more than 9-nm thick to accommodate the mean length of *E. coli* glycan strands (10). Density profiles (Fig. S1) taken along vectors normal to the *E. coli* and *C. crescentus* saccular side walls in the tomograms showed that Gram-negative peptidoglycan is at most 4-nm thick. Similar density profiles of the peptidoglycan layer in intact *C. crescentus* cell tomograms showed a slightly larger thickness (≤7 nm), probably reflecting the presence of proteins embedded in the sacculi of intact cells and the larger defocus used for the whole-cell tomograms. These results agree well with previous AFM measurements of hydrated *E. coli* sacculi (11) and EM images of thin-sectioned, vitrified *E. coli* cells (12), respectively, but none of the above are compatible with the Scaffold model.

Earlier small-angle neutron scattering experiments suggested that *E. coli* peptidoglycan (13) was mostly single-layered (with a thickness of 2.5 nm), but could be up to three layers (7-nm) thick. Additional density profiles of our tomograms along the side walls as well as *C. crescentus* stalks and *E. coli* poles showed that the purified sacculi were uniformly thick (Fig. S2). Views of the *C. crescentus* side wall sometimes revealed a single row of tubular densities (Fig. 2 *C* and *D* and Movie S1), but never double rows, which together with the thickness measurements support a model in which peptidoglycan is single-layered everywhere. It is likely that sacculi in the earlier neutron-scattering experiments appeared multilayered because they were clumped together. Indeed, aggregated (1) and stacked sacculi (14) were frequently observed in our preparations.

Sacculi Are Not Stretched Circumferentially. It is widely reported in the literature that the peptidoglycan is "stretched" because of cytosolic turgor, as evidenced by light microscope images of SDS-treated *E. coli* cells, which contracted along their polar axis because of the loss of cytosolic turgor (15). Whether or not there were also small changes in cell diameter, however, could not be resolved. When we compared our in vitro sacculi, which are in an unstretched state, to the in situ sacculi in our previous cryotomograms of intact *C. crescentus* cells (16) (Fig. S3), no significant differences in circumference at the widest point of the cell were found. Corresponding comparisons of cellular lengths were not done because cells grow by elongation, and differences because of stretching would have been confounded by cell growth. Assuming that *C. crescentus* and *E. coli* sacculi have

Author contributions: L.G. and G.J.J. designed research; L.G. and S.C. performed research; L.G., S.C., and G.J.J. analyzed data; and L.G. and G.J.J. wrote the paper.

The authors declare no conflict of interest.

This article is a PNAS Direct Submission.

[1]To whom correspondence should be addressed. E-mail: jensen@caltech.edu.

This article contains supporting information online at www.pnas.org/cgi/content/full/0808035105/DCSupplemental.

MICROBIOLOGY

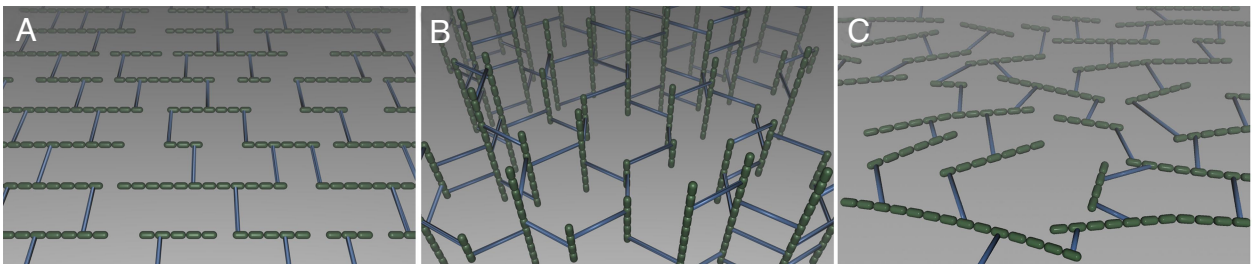

Fig. 1. Models of peptidoglycan organization. The Layered (*A*), Scaffold (*B*), and Disorganized Layered (*C*) models are viewed obliquely to the sacculus surface and toward the cell pole. Disaccharides (green pills) are approximately 1-nm long and the stretched peptide crosslinks (blue sticks) are approximately 4 nm long. The length distribution of the glycan strands (3-mers to 14-mers) approximates the resolvable part of HPLC chromatograms of purified, hydrolyzed sacculi (10), and the crosslinkage is kept less than the experimentally determined maximum of 50% (21). It is not known whether glycans run parallel or antiparallel to each other.

conserved mechanical properties, the early light microscopy data and our electron tomographic data together indicate that cytosolic turgor stretches sacculi along their polar axis but not around their circumference. This observation, as well as the thinness of the sacculus and the orientation of the wrinkles, all point to a circumferential Layered model (Fig. 1*A*) where the glycans lie in the plane of the cell wall perpendicular to the polar axis, since peptides are expected to be more flexible than glycans and would then be negotiating the shrinkage and wrinkles.

Interpretation of Cryotomographic Densities. In further support of this model, close-up views of *C. crescentus* and *E. coli* sacculi revealed numerous thin tubes of density mostly in the plane of the sacculus and roughly perpendicular to the long axis of the cell (Figs. 2–4 *Insets* and Movie S1 and Movie S2). Because (i) after purification the sacculi are composed of only glycans and peptides, (ii) glycans are bulkier than peptides and will therefore be more prominent in tomograms than peptides, and (iii) many tubes were longer than peptide crosslinks [which are ≤4 nm when stretched (8)], we conclude that the majority of the tubes seen represented glycans. The striking uniformity of the tubes and the absence of any features that would have suggested bundling, like for instance wide gaps next to unusually thick tubes, suggested that the tubes were in fact single glycans rather

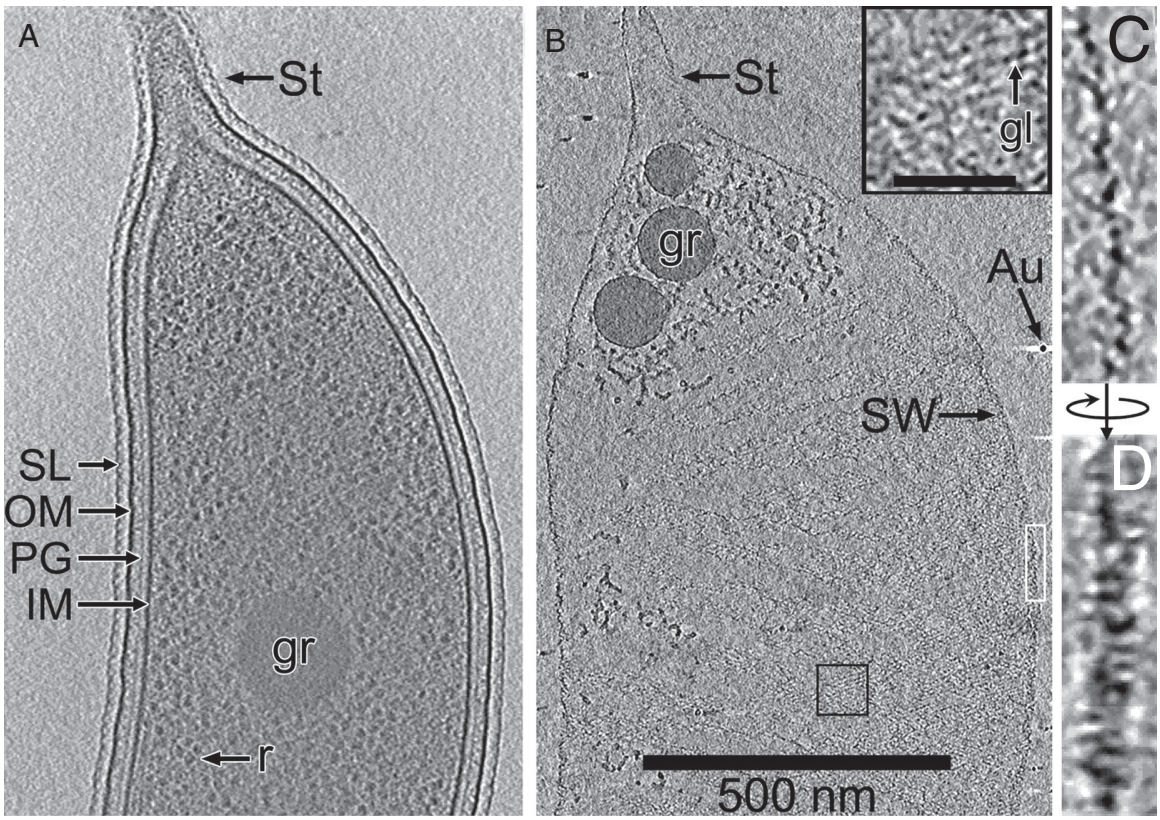

Fig. 2. Comparison of in situ and in vitro sacculi. (*A*) Twenty-five-nm thick Z-slice through the 3-D reconstruction of a *C. crescentus* CB15N cell. (*B*) 10-nm thick Z-slice through the 3-D reconstruction of a purified sacculus. Both panels are at the same scale. Abbreviations: (SL) S-layer; (OM) outer membrane; (PG) peptidoglycan layer, that is, the sacculus; (IM) inner membrane; (r) ribosome-like particle; (St) stalk; (Au) gold fiducial; (gr) granule; (gl) glycan strand; (SW) side wall. (*Inset*) Close-up of sacculus showing glycan strands. Note that the highly flexible sacculus has flattened because of the surface tension of the thin aqueous film, so that it appears wider than the intact cell. The cell tomogram is from reference (16). (*C*) Enlarged view (4-nm thick slice) showing the glycan strands in the sacculus side wall boxed in white in (*B*). (*D*) The same glycan strands as in (*C*), rotated approximately 90° around the vertical axis.

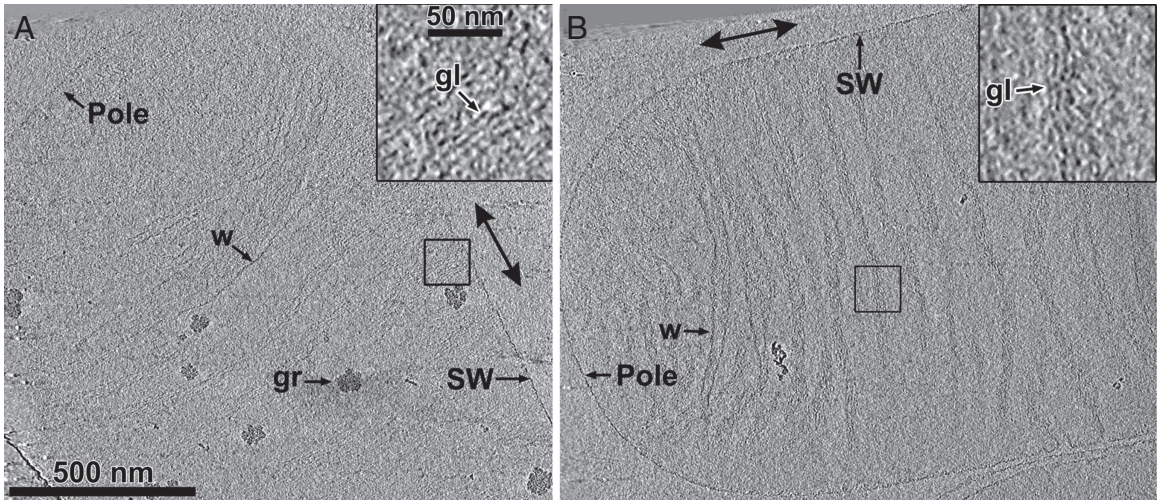

Fig. 3. Tomographic slices of *E. coli* sacculi. Ten-nm thick Z-slices of *E. coli* strain MG1655 (*A*) and XL-10 sacculi (*B*). Abbreviations are the same as in Fig. 2 except for: (w) wrinkle. The double-headed arrow denotes the saccular polar axis. (*Insets*) Four-fold enlarged views of the boxed regions. Note that the direction of the strand densities is approximately perpendicular to the saccular polar axis. Compared to *C. crescentus*, *E. coli* sacculi images had poorer contrast, which may be a result of the ice surrounding *E. coli* sacculi being at least 20 nm thicker.

than bundles (see Movie S1 and Movie S2). The tubes were, however, thicker (≈4 nm) and more elliptical than individual glycans (≈1 nm), but such widening and distortion would be expected because of the low-pass filter and missing "wedge" inherent in the imaging system's point spread function. Although others have already demonstrated that electron cryomicroscopy can resolve slender polymers such as purified double-stranded DNA (≈2.5-nm thick) in 2-D (17) and 3-D (18), we believe that the visualization of the even thinner individual glycans here was facilitated by the thinness of the ice (<100 nm), the very low salt content of the buffer (<10 mM sodium phosphate), the large defocus (−6 μm), and the use of an ultra-sensitive lens-coupled

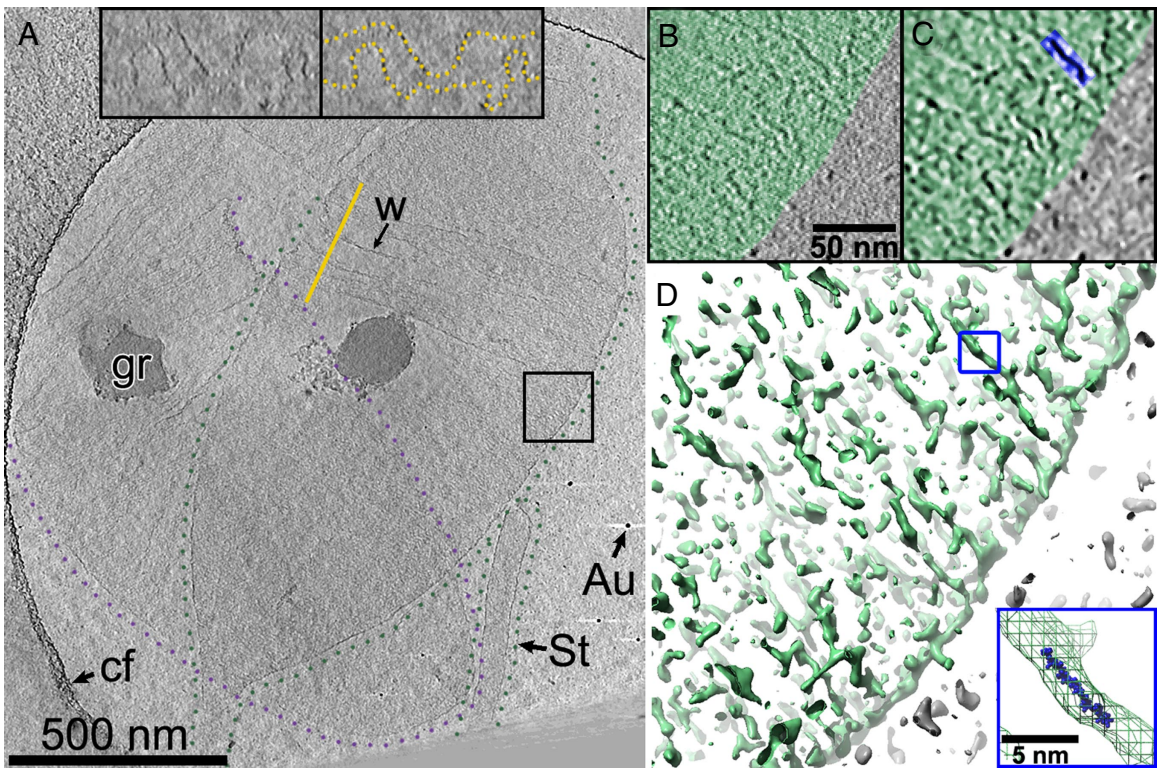

Fig. 4. Details of peptidoglycan organization. (*A*) 30-nm thick Z-slice of two overlapping *C. crescentus* CB15N sacculi, outlined by green or violet dotted lines. Abbreviations are the same as in Figs. 3 and 3 except for: (cf) carbon support film. (*Insets*) 30-nm thick cross-sections cut through the yellow line in the main panel. The yellow dotted line follows the ''upper'' and ''lower'' halves of the peptidoglycan. (*B*) Enlarged view (4-nm thick slice) of the sacculus side wall boxed in (*A*). (*C*) Image (*B*) after 3-D median filtration; one putative glycan strand is highlighted in blue. The green-shaded region demarcates the peptidoglycan. (*D*) Isosurface rendering the volume shown in (*C*). The putative glycan strand in (*D*) is boxed in blue. The noise densities outside of the sacculus are colored gray for clarity. (*Inset*) Superposition of glycan 9-mer atomic model in the blue-boxed density, shown for a sense of scale.

CCD. Indeed simulated tomograms of glycans under the same imaging conditions supported the interpretation that the tubes were individually resolved strands (Fig. S4).

It is important to note, however, that the high-energy electrons used to produce the image break covalent bonds, deposit energy, and cause local atomic rearrangements despite the sample's frozen state (19, 20). To minimize this damage, low doses are used and tomograms have correspondingly low signal-to-noise ratios (SNRs). Thus because of these two factors (specimen damage and low SNRs), small bumps, kinks, branches, and apparent connecting densities may not be reliable, and should not be interpreted as specific conformations of glycans or peptide crosslinks. Moreover, such conformational details probably change considerably when the sacculi collapse. Nor can the lengths, number, or identity (glycan, peptide, or noise) of particular densities be confidently measured or assigned. What is clear is that the majority of the strongest, most-continuous densities in the collapsed sacculi (which must be glycans) form a single layer of remarkably consistent thin tubes that lie in the plane of the sacculi roughly perpendicular to the polar axis. This pattern was evident in both *E. coli* and *C. crescentus* and regardless of the angle the sacculus made with the tilt axis, confirming that it was not an artifact created by the missing wedge of data (Fig. S5 and Fig. S6). The architecture of the strands was as far as we could tell uniform along the sidewalls of the cell (i.e., no "seams" or "growth-zones" were discerned).

Sacculi Are Poorly Ordered. Previous X-ray scattering experiments of sacculus solutions done by us (Fig. S7) and others (14) failed to reveal dominant spacings. Likewise the density tubes visualized here in tomograms were not regularly spaced or perfectly parallel (Fig. 4 *B* and *C*). Nevertheless because the two halves of individual sacculi were computationally separable in the 3-D tomograms, we were able to extract and Fourier transform small patches of *C. crescentus* peptidoglycan. These transforms revealed that there was more power parallel to the saccular polar axis than perpendicular to it (Fig. S8 and Fig. S9 *C* and *D*), confirming that although poorly ordered, the glycan strands must be mostly circumferential. In agreement with the Fourier analyses, images like Fig. 2 *C* and *D* showed that glycan strand separations typically ranged from approximately 5–8 nm. *E. coli* glycan strands appeared more parallel than those of *C. crescentus*, but there were no patches flat enough to calculate meaningful transforms (see Movie S1, Movie S2, Fig. 3, Fig. S4, and Fig. S5). Purified sacculi are therefore noncrystalline as seen in SAXS patterns from sacculi solutions and in Fourier transforms of patches of individual sacculi, but the glycan strands could be readily identified because of their nonrandom, circumferential direction. Whereas it is possible that peptidoglycan under pressure within living cells is more ordered, we think it can't be dramatically so because glycan strands have a broad length distribution (10) and the peptide crosslinks have diverse structures (21).

Thus our images support a Disordered Circumferential Layered model (Fig. 1*C*) wherein a single layer of linked glycan strands encircle the cell in a disorganized hoop-like fashion, like that drawn earlier by Verwer and Schwarz (4) and others. The structural difference between a Crystalline Layered model (like that routinely shown in current textbooks) and a Disordered Layered model is not trivial. A crystalline sacculus could be extended indefinitely with no other guiding scaffold other than its own strands (just like a crystal lattice templates its own growth), for instance by a peptidoglycan polymerase holoenzyme that replaced any existing glycan strand with three new strands oriented in exactly the same direction, as proposed in the "three-for-one" replicase model (22). Instead, the disorder seen here and a growing body of other evidence now suggests that extrinsic factors like cytoskeletal filaments are essential to guide the peptidoglycan synthesis machinery and determine cell shape (23).

Materials and Methods

Specimen Preparation. Sacculi from *C. crescentus* strain CB15N and *E. coli* strains MG1655 and XL-10 were prepared by using a published protocol (24). A 1-liter cell culture was grown to mid-exponential phase ($OD_{600} \approx 0.2–0.4$) in PYE (*C. crescentus*) or LB (*E. coli*). The cells were chilled on ice for 10 min and then pelleted at 4 °C at 4,930 × *g* for 15 min. The supernatant was removed and the cells were resuspended in 12 ml ice-cold ddH_2O (*C. crescentus*) or 100 mM NaCl (*E. coli*). A stir-bar and 12 ml high-purity 4% wt/vol SDS were added to a 100-ml volumetric flask and then preheated to 80–90 °C in a water bath. The resuspended cells were added to the hot SDS, drop-by-drop, over a period of 30 min. Another 12 ml hot 8% SDS was added, and then the entire mixture was stirred at 80–90 °C for 1 h. The SDS was washed away by three rounds of pelleting (43,223 × *g*) and resuspension in ddH_2O. Nucleic acids were digested by using DNase I and RNase, and then proteins were digested overnight with trypsin (the peptide crosslinks do not have any trypsin cleavage sites). The enzymes were denatured with 4% SDS at 80–90 °C and separated from the sacculi by pelleting at 43,223 × *g* for 30 min. The SDS was removed by three rounds of pelleting and resuspension in ddH_2O. The sacculi were then resuspended in 10 mM sodium phosphate buffer, pH 7.0. Sacculi were combined with a 5-fold-concentrated mixture of BSA-treated 5-nm and 10-nm colloidal gold beads. A 3-μl gold-and-sacculi drop was applied manually to the carbon side of a plasma-cleaned C-flat CF222C grid (*C. crescentus*) or a CF422C grid (*E. coli*). The grids were plunge-frozen in liquid propane/ethane (67%:33% by volume) (25) by using a Vitrobot (FEI Inc.). Grids were stored in liquid nitrogen until use.

Small Angle X-Ray Scattering. Solution X-ray scattering data were recorded at SSRL Beamline 4–2 and ALS Beamline 12.3.1. The X-ray wavelength was 1.38 Å (SSRL) or 1.03 Å (ALS). The sample-to-detector distance ranged from 1.6–2.5 m. Circular averaging, intensity scaling and background subtraction, and radial averaging were done by using either *MarParse* (26) or *Ogre*. Samples were loaded into sample cells with mica windows and kept at 20–22 °C.

Tomography Data Collection. All specimens were imaged in a FEI "Polara" transmission electron cryomicroscope equipped with a FEG operating at 300 kV. The electron image was energy-filtered by using a 20-eV slit. Tilt series were acquired by using the program UCSF Tomography (27). The tomogram quality was optimized by screening a large number of imaging conditions. The best tomograms were obtained by using 22,500× magnification, 6-μm underfocus, 100 electrons/Å^2 total dose, ±70° total tilt, and 1.5–2° increments. Specimens were dosed by using either the 1/cosine scheme and or the exponential scheme with a Λ value of 50–100 nm (28), which approximates the thickness of the vitreous ice. Images were collected on a 4 k × 4 k, lens-coupled Gatan UltraCam CCD camera, hardware-binned by 2, which yielded a pixel size of 0.78 nm (27,500× mag.) or 0.96 nm (22,500× mag.) at the specimen level. In total, 62 *C. crescentus* CB15N, 30 *E. coli* MG1655, and 18 *E. coli* XL-10 tilt series were acquired. Approximately 10% of the resulting tomograms were of sufficient quality to reveal glycan strands in 10-nm thick Z-slice averages, and only 5 of the *C. crescentus* tomograms revealed the glycan strands in 1-nm thick slices.

Image Processing. The ice around some sacculi was so thin that the mean image intensities approximately doubled at high tilts when the 1/cosine dose scheme was used. To compensate in those cases, the images were mass-normalized by using the IMOD densnorm program (29). The tilt series were 2-D low-pass filtered to attenuate the spatial frequencies higher than the first CTF zero. Tilt series alignment and weighted back-projection were done with IMOD. Because of the thinness of the ice, the image intensities were used without first taking the log; the resulting tomograms had fewer "streaking" artifacts that could be detected by viewing the gold fiducials along the tilt axis.

To determine the thickness of the sacculi, a small patch of a 3-D median-filtered tomogram was segmented by using 3dmod (29) and then the density values of the *unfiltered* tomogram were integrated along vectors normal to the segmentation by using an in-house program.

To generate the isosurfaces shown in Movie S1 and Movie S2, the densities were thresholded at a level high enough (density values from −6505 to −700) to filter out the noisy buffer densities. Gold fiducial and BSA (used to solubilize the gold) densities were removed manually. Most of the remaining densities had a tube-like appearance, but were obfuscated by smaller densities that could be short glycans, peptides, or noise. Density islands <500 voxels were removed, which corresponds to glycans shorter than ≈25 nm, assuming that glycan strands are tubes that have a 4 × 8 nm voxel^2 X–Z cross-section. Because the thresholding generated features smaller than the resolution limit, the isosurface was smoothed with a Gaussian filter.

Power spectra of 2-D sections were calculated by using ImageJ (http://rsb.info.nih.gov/ij/).

Circumference Measurement. To increase the contrast, the tomograms of CB15N cells and sacculi were binned to a final pixel size of ≈2.4 nm and then denoised by 3-D median filtration. All tomograms were rotated to a common view along the sacculus polar axis and centered on the widest part of the side wall by using the IMOD ''slicer'' utility. The circumferences of the flattened, purified sacculi were estimated as the length of 2 parallel lines connected by small semicircles at their ends. The circumferences of tubular in situ sacculi were estimated as the perimeter of an ellipse. The vertical distance (semiminor axis) across the cell (from the "upper" to the "lower" halves of peptidoglycan layer, where the missing wedge obscures horizontal details) was ascertained from differences in texture between the cytoplasm and periplasm.

Tomogram Simulation. Glycan strand coordinates (8) were arranged by using UCSF Chimera (30) as shown in Fig. S4. All subsequent simulations were done with Bsoft (31) by using imaging parameters close to the optimized experimental conditions. Briefly, a 3-D map was generated by using a 0.096-nm voxel and then projected as a tilt series by using a ±69° total tilt, and 1.5° tilt increment. The tilt series were then corrupted with a 6-μm underfocused CTF and then resampled by using a 0.96-nm pixel. Tomograms were reconstructed by using IMOD using the same settings as for the real data.

Fig. 1 was made with blender (http://www.blender.org). Figs. 2–4 *A–C*, S5, and S6 were made with the IMOD slicer utility (29). Fig. 4*D* was made with the UCSF Chimera package (30). Fig. S8 and Fig. S9 *A–C* were made by using ImageJ. Figs. S1–S3, S7, S8*D*, and S9*D* were made by using Microsoft Excel and Kaleidagraph (Synergy Software). The Movie S1 and Movie S2 frames were rendered with Amira (Mercury Computer Systems, Inc.), edited with Adobe Photoshop, spliced and encoded by using Adobe Premiere, and compressed with Apple QuickTime Pro.

ACKNOWLEDGMENTS. We thank Drs. W. F. Tivol for help with EM; H. Tsuruta and M. Hammel for help at beamlines SSRL 4-2 and ALS 12.3.1, respectively; A. Briegel, D.P. Dias, and Z. Li for sharing data; J. Skerker, K.C. Huang, N. Wingreen, and P. Leong for discussions; and Mr. Everett Kane (SuperSoft Design, New York, NY) for Fig. 1C. This work was supported in part by National Institutes of Health Grants R01 AI067548 and P50 GM082545 to G.J.J., a Searle Scholar Award to G.J.J., the Beckman Institute at Caltech, and gifts to Caltech from the Gordon and Betty Moore Foundation and the Agouron Institute. L.G. is a Damon Runyon Fellow supported by a fellowship from the Damon Runyon Cancer Research Foundation (DRG-1940-07).

1. Formanek H, Formanek S (1970) Specific staining for electron microscopy of murein sacculi of bacterial cell walls. *Eur J Biochem* 17:78–84.
2. Dietrich I, Formanek H, Fox F, Knapek E, Weyl R (1979) Reduction of radiation-damage in an electron-microscope with a superconducting lens system. *Nature* 277:380–381.
3. De Petris S (1967) Ultrastructure of the cell wall of *Escherichia coli* and chemical nature of its constituent layers. *J Ultra Res* 19:45–83.
4. Verwer RWH, Nanninga N, Keck W, Schwarz U (1978) Arrangement of glycan chains in sacculus of *Escherichia coli*. *J Bacteriol* 136:723–729.
5. Dmitriev BA, *et al*. (2003) Tertiary structure of bacterial murein: The scaffold model. *J Bacteriol* 185:3458–3468.
6. Dmitriev B, Toukach F, Ehlers S (2005) Toward a comprehensive view of the bacterial cell wall. *Trends Microbiol* 13:569–574.
7. Vollmer W, Holtje JV (2004) The architecture of the murein (peptidoglycan) in gram-negative bacteria: Vertical scaffold or horizontal layer(s)? *J Bacteriol* 186:5978–5987.
8. Meroueh SO, *et al*. (2006) Three-dimensional structure of the bacterial cell wall peptidoglycan. *Proc Natl Acad Sci USA* 103:4404–4409.
9. Jensen GJ, Briegel A (2007) How electron cryotomography is opening a new window onto prokaryotic ultrastructure. *Curr Opin Struct Biol* 17:260–267.
10. Harz H, Burgdorf K, Holtje JV (1990) Isolation and separation of the glycan strands from murein of *Escherichia coli* by reversed-phase high-performance liquid-chromatography. *Anal Biochem* 190:120–128.
11. Yao X, Jericho M, Pink D, Beveridge T (1999) Thickness and elasticity of gram-negative murein sacculi measured by atomic force microscopy. *J Bacteriol* 181:6865–6875.
12. Matias VRF, Al-Amoudi A, Dubochet J, Beveridge TJ (2003) Cryo-transmission electron microscopy of frozen-hydrated sections of *Escherichia coli* and *Pseudomonas aeruginosa*. *J Bacteriol* 185:6112–6118.
13. Labischinski H, Goodell EW, Goodell A, Hochberg ML (1991) Direct proof of a more-than-single-layered peptidoglycan architecture of *Escherichia coli* W7: A neutron small-angle scattering study. *J Bacteriol* 173:751–756.
14. Burge RE, Fowler AG, Reaveley DA (1977) Structure of peptidoglycan of bacterial-cell walls. 1. *J Mol Biol* 117:927–953.
15. Koch AL, Lane SL, Miller JA, Nickens DG (1987) Contraction of filaments of *Escherichia coli* after disruption of cell-membrane by detergent. *J Bacteriol* 169:1979–1984.
16. Briegel A, *et al*. (2006) Multiple large filament bundles observed in *Caulobacter crescentus* by electron cryotomography. *Mol Microbiol* 62:5–14.
17. Amzallag A, *et al*. (2006) 3D reconstruction and comparison of shapes of DNA minicircles observed by cryo-electron microscopy. *Nucleic Acids Res* 34:e125.
18. Vos MRJ, *et al*. (2007) Insights in the organization of DNA-surfactant monolayers using cryo-electron tomography. *J Am Chem Soc* 129:11894–11895.
19. Iancu CV, Wright ER, Heymann JB, Jensen GJ (2006) A comparison of liquid nitrogen and liquid helium as cryogens for electron cryotomography. *J Struct Biol* 153:231–240.
20. Wright ER, Iancu CV, Tivol WF, Jensen GJ (2006) Observations on the behavior of vitreous ice at similar to 82 and similar to 12K. *J Struct Biol* 153:241–252.
21. Glauner B, Holtje JV, Schwarz U (1988) The composition of the murein of *Escherichia coli*. *J Biol Chem* 263:10088–10095.
22. Holtje JV (1998) Growth of the stress-bearing and shape-maintaining murein sacculus of *Escherichia coli*. *Micro Mol Bio Rev* 62:181–203.
23. Cabeen MT, Jacobs-Wagner C (2005) Bacterial cell shape. *Nat Rev Microbiol* 3:601–610.
24. Poindexter JS, Hagenzieker JG (1981) Constriction and septation during cell-division in caulobacters. *Can J Microbiol* 27:704–719.
25. Tivol WF, Briegel A, Jensen GJ (2008) An improved cryogen for plunge freezing. *Microsc Microanal* 14:375–379.
26. Smolsky IL, *et al*. (2007) Biological small-angle x-ray scattering facility at the Stanford synchrotron radiation laboratory. *J Appl Crystallogr* 40:S453–S458.
27. Zheng QXS, Braunfeld MB, Sedat JW, Agard DA (2004) An improved strategy for automated electron microscopic tomography. *J Struct Biol* 147:91–101.
28. Grimm R, *et al*. (1998) Electron tomography of ice-embedded prokaryotic cells. *Biophys J* 74:1031–1042.
29. Mastronarde DN (1997) Dual-axis tomography: An approach with alignment methods that preserve resolution. *J Struct Biol* 120:343–352.
30. Pettersen EF, *et al*. (2004) UCSF chimera - A visualization system for exploratory research and analysis. *J Comput Chem* 25:1605–1612.
31. Heymann JB, Cardone G, Winkler DC, Steven AC (2008) Computational resources for cryo-electron tomography in Bsoft. *J Struct Biol* 161:232–242.